A Comparison of Monolithic and Layered-Plate Configurations for Containment

Thomas J. Vasko, PhD, PE

Central Connecticut State University
New Britain, CT

Abstract

Jet-engine fan, compressor, and turbine blades require containment cases to ensure that any released blade fragments are contained within the engine and do not penetrate the case, where they can damage critical engine components or penetrate the passenger cabin. To determine the centrifugal strength of turbomachinery rotors, disk-burst tests are performed in vertical-axis spin pits that require containment cases to ensure the safety of the surrounding test area. In these applications, the containment cases are sized to determine the minimum thickness the case must have in order to contain all rotating-part fragments. The current study compares a monolithic plate with various layered-plate configurations to assess containment capability as determined by the perforation velocity, the lowest projectile velocity that completely penetrates the target. The targets include a monolithic plate and several layered-plate configurations with and without gaps. The projectile is a rigid sphere that impacts the target normal to the surface. The target plates are made of titanium-6Al-4V that is modeled using the MAT_TABULATED_JOHNSON_COOK (MAT_224) constitutive model in LS-DYNA®. This is an elastic viscoplastic material model with strain rate and temperature-dependent stress versus strain curves. In addition, plastic failure strain is defined as a function of triaxiality and Lode parameter, strain rate, temperature, and element size. Results of the study can be used to determine the optimum containment-case configuration for a variety of high-speed rotating components.

Introduction

Jet-engine fan, compressor, and turbine blades require containment cases to ensure that any released blade fragments are contained within the engine and do not penetrate the case, where they can damage critical engine components or penetrate the passenger cabin. To determine the centrifugal strength of turbomachinery rotors, impellers, and flywheels, disk-burst tests are performed in vertical-axis spin pits that also require containment cases to ensure the safety of the surrounding test area. In all these applications, the containment cases are sized to determine the minimum thickness the case must have to contain all rotating-part fragments.

Analytical approaches for the design of containment cases, such as those used by Hagg and Sankey [1] in the design of cylindrical-shell containment systems for turbine rotors, use energy- and momentum-transfer principles. In these approaches, the kinetic energy of the projectile to be contained is absorbed by the strain energy of the target. Although these energy approaches have been shown to correlate with test data, their applicability to a wide range of geometries and materials—as well as their ability to accurately capture friction, strain rate and temperature effects, local stress concentrations, fracture, and a range of failure modes—is limited.

A more robust approach in designing containment cases is to use the finite-element method. The finite-element method not only allows a broader range of geometry and materials to be investigated, but also allows friction, strain-rate, and temperature effects, as well as a range of

failure models to be readily incorporated in the containment-case design. Stamper and Hale [2] showed good correlation to the failure modes in the tests of Hagg and Sankey using LS-DYNA® finite-element analyses. Hu, Wu, and Guo [3] used the Element Free Galerkin (EFG) method in LS-DYNA to predict the dynamic fracture and crack growth in the ductile material for an engine impeller under impact loads. Kelly, Pereira, Revilock, and Matheny [4] also used the finite-element method in LS-DYNA to compare a flat plate to a plate with a surface curved outward from the projectile, where they demonstrated an improved containment capability for the curved plate with analysis that was also correlated with test data.

The purpose of the current work is to explore the possibility that layered structures could provide an increased containment capability, thus reducing the cost and weight for large spin-rig containment structures. The objective is to determine if a substantial improvement in perforation velocity can be achieved with a layered configuration to warrant additional, more detailed study and a rigorous and expensive test program for validation.

The current study investigates normal impact of a rigid spherical projectile to determine the perforation velocity, the lowest velocity to completely penetrate the target, for several layered-target configurations. The target configurations have been selected to answer the fundamental question of whether a single monolithic structure of a specific thickness is a better containment structure than a layered structure with the same total thickness and, in addition, to what extent gaps between layers affect the perforation velocity.

Analysis Models

The projectile is a rigid steel sphere with a three-inch diameter that impacts the target plate normal to the surface. The steel properties include a modulus of 27.557E6 psi, a Poisson Ratio of 0.27, and a density of 7.35E-4 lb-sec^2/in^4.

The targets consist of various configurations of 48-inch square titanium-6Al-4V plates with thicknesses of two inches, one inch, and one-half inch that have no applied boundary conditions. A consistent 0.125-inch mesh size for all elements in each of the target plates was also used. Constant-stress solid elements were used for both the projectile and the targets. Frictionless contact between the projectile and the target was defined using the ERODING_SINGLE_SURFACE contact option, and segment-based contact using the SOFT=2 constraint option was also defined.

Five different configurations of the target plates were analyzed. Case 1 is a monolithic two-inch target. Cases 2 and 3 each have a total thickness of two inches; however, Case 2 consists of two one-inch-thick plates and Case 3 consists of four half-inch-thick plates, and, in both cases, no gaps exist between the plates. Cases 4 and 5 use plates that have a total thickness of two inches, but there are gaps between the target plates that make the total thickness greater than two inches. Case 4 uses two one-inch plates with a half-inch gap between the plates for a total thickness of 2.5 inches, and Case 5 uses four half-inch plates with a quarter-inch gap between the plates for a total thickness of 2.75 inches. Figure 1 shows the cross-section view of the projectile and target configurations for each of the five cases analyzed.

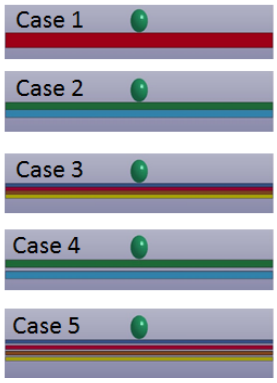

Case	Number of Plates	Plate Thickness (in)	Gap Between Plates (in)	Total Thickness (in)
1	1	2.00	No Gap	2.00
2	2	1.00	No Gap	2.00
3	4	0.50	No Gap	2.00
4	2	1.00	0.50	2.50
5	4	0.50	0.25	2.75

Figure 1: Cross-Section Views for Layered Configurations Analyzed

The target material is titanium-6Al-4V that was modeled using the MAT_TABULATED_JOHNSON_COOK (MAT_224) constitutive model. The theoretical development of this model and the specific inputs for the titanium-6Al-4V material were developed in a collaborative effort of the Federal Aviation Administration (FAA), the National Aeronautics and Space Administration (NASA), Ohio State University (OSU), George Washington University (GWU), and George Mason University (GMU) [5-8]. The details are provided in References 5-8, and an overview of the material model is provided in the next section.

Titanium-6Al-4V Material Model Overview

The titanium-6Al-4V was modeled using the MAT_TABULATED_JOHNSON_COOK material model input. This material model is an isotropic elastic thermo-viscoplastic constitutive relation where stress is a function of strain, strain rate, and temperature:

$$\sigma_{ij} = \sigma_{ij}(\varepsilon_{ij}, \dot{\varepsilon}_{ij}, T)$$

where σ_{ij} is stress, ε_{ij} is strain, $\dot{\varepsilon_{ij}}$ is strain rate, and T is temperature. Tensile tests were conducted at various strain rates and temperatures to derive the input stress-strain curves and tables. In the plastic region, the material response is determined by a von Mises yield surface that expands or contracts due to strain hardening, rate effects, and thermal softening.

To model accumulated damage and element failure using solid elements, four input parameters are defined: (1) a table of curves that defines the plastic failure strain as a function of triaxiality and Lode parameter, which results in the definition of a failure surface; (2) a load curve that defines the plastic failure strain as a function of plastic strain rate; (3) a load curve that defines the plastic failure strain as a function of temperature; and (4) a load curve that defines that plastic failure strain as a function of element size.

Triaxiality is defined by the equation:

$$\tau = \frac{p}{\sigma_{vm}}$$

where p is the pressure, and σ_{vm} is the Von Mises stress, and the Lode parameter is defined by the equation:

$$\theta_L = \frac{27\, s_1 s_2 s_3}{2\sigma_{vm}^3}$$

where s_1, s_2, and s_3 are the principal deviatoric stresses. The Lode parameter ranges between plus and minus one, which bounds the failure surface. The plastic failure strain is defined by:

$$\varepsilon_{pf} = f(\tau, \theta_L)\; g(\dot{\varepsilon}_p) h(T) i(l_c)$$

where τ is the triaxiality, θ_L is the Lode parameter, $\dot{\varepsilon}_p$ is the plastic strain rate, and l_c is the element size. When more than one of the failure parameters is used, the net plastic failure strain is the product of the functions defined in the above equation.

The failure criterion is based on an accumulated-damage parameter defined by:

$$F = \int \frac{\dot{\varepsilon}_p}{\varepsilon_{pf}} dt$$

where $\dot{\varepsilon}_p$ is the plastic strain rate, and ε_{pf} is the plastic failure strain that changes continuously as a function of the triaxiality and Lode parameter. When this damage parameter is greater than or equal to one, the element has failed and is deleted.

To determine the failure surface, various material specimens each with a unique triaxiality and Lode parameter representing a specific point on the failure surface were created and tested. Using the triaxiality, Lode parameter, and failure-strain data from that specimen testing, a complete failure surface is then generated.

Strain-rate and temperature testing series were then completed to determine the load curves with the failure-strain scale factors for various strain rates and temperatures. Finally, by varying the size of the elements in the mesh analytically, a load curve that accounts for many different mesh sizes was created.

In his report, Haight [8] provides details of the material-model input-parameter development, including the failure surface generation for the titanium-6Al-4V material used in this analysis. The complete input-data set for the titanium model used in the analyses is also available on the Aerospace Working Group Webpage (awg.lstc.com) under the Resources menu and Material Input Parameter Submenu.

Perforation Velocity

The objective of the analyses is to determine the perforation velocity for each of the five cases to determine which configuration provides the most effective containment capability. The perforation velocity is defined as the lowest velocity at which there are failures through all the layers so that when viewed from the bottom layer (the opposite side from where the projectile first impacts) with all the layers present, the projectile can be seen; i.e., there is a hole (caused by failed elements) through all the layers. Therefore, the layered-plate configuration with the largest perforation velocity would provide the most containment capability.

Results

The results for the five cases analyzed are presented in Table 1. The results show that Case 2, with two one-inch-thick plates and no gap between the plates, has the highest perforation velocity and, therefore, is the best configuration for containment. Going from a single two-inch-thick plate (Case 1) to two one-inch plates (Case 2) resulted in the perforation velocity increasing 9.4% from 18170 in/s to19870 in/s. This trend, however, did not continue, because the four half-inch plates (Case 3) have a perforation velocity of 16660 in/s, which is less than that of both the single two-inch plate (Case 1) and the two half-inch plates (Case 2). The cases with gaps—Case 4, with two one-inch-thick plates and a one-inch gap, and Case 5, with four half-inch plates and a quarter-inch gap—have the lowest perforation velocities.

Case	Number of Plates	Plate Thickness (in)	Gap Between Plates (in)	Total Thickness (in)	Perforation Velocity (in/s)
1	1	2.00	No Gap	2.00	18170
2	**2**	**1.00**	**No Gap**	**2.00**	**19870**
3	4	0.50	No Gap	2.00	16660
4	2	1.00	0.50	2.50	16110
5	4	0.50	0.25	2.75	16100

Table 1: Perforation-Velocity Results

Contour plots of the through-thickness (z-displacement) and the effective plastic strain in the impact region as viewed from the bottom layer are shown for each of the cases in Figures 2 through 6. Table 2 summarizes those results by comparing the maximum through-thickness displacement and maximum plastic strain for each case along with the perforation velocity. Case 5, with the lowest perforation velocity, had the highest plastic strain and the largest displacement, while Case 2, with the highest perforation velocity, had the next highest plastic strain and displacement. These results do not appear to indicate any specific trend, nor is it readily apparent from these results why Case 2 had the highest perforation velocity.

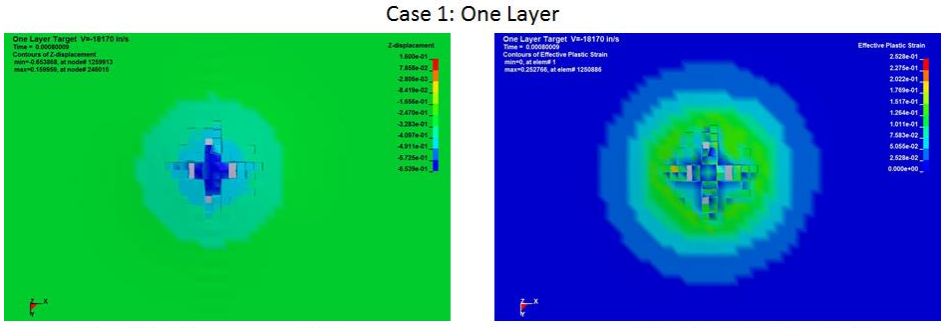

Figure 2: Case 1 Impact Region Out-of-Plane Displacement and Plastic Strain

Case 2: Two Layers

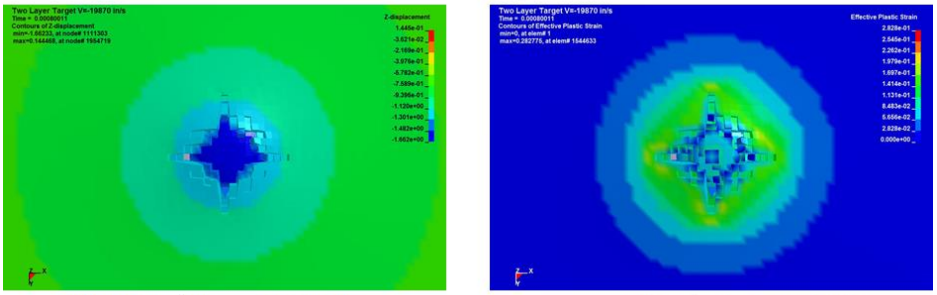

Max Z-Displacement=1.662 in | Max Plastic Strain=28.28

Figure 3: Case 2 Impact Region Out-of-Plane Displacement and Plastic Strain

Case 3: Four Layers

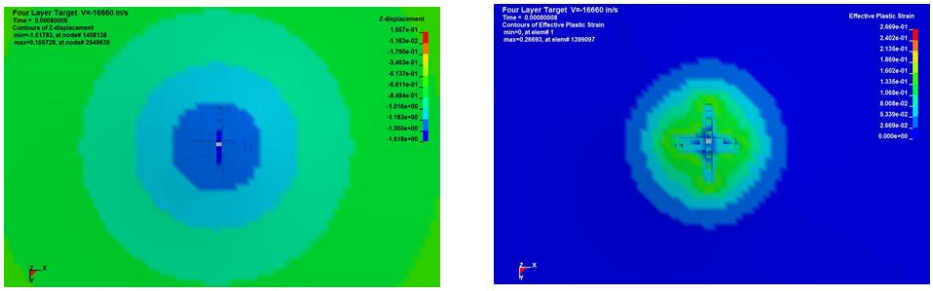

Max Z-Displacement=1.518 in | Max Plastic Strain=26.69

Figure 4: Case 3 Impact Region Out-of-Plane Displacement and Plastic Strain

Case 4: Two Layers with a Half-Inch Gap

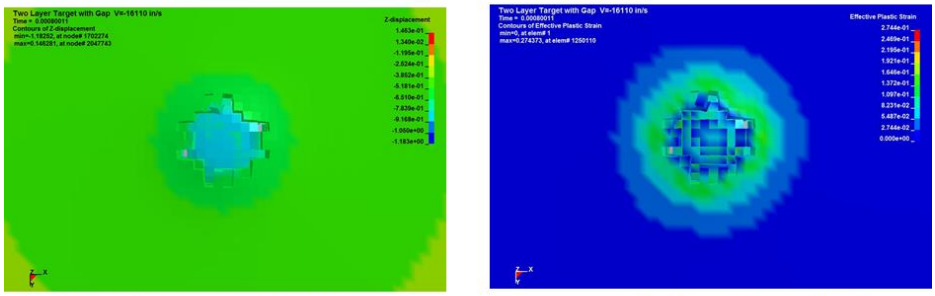

Max Z-Displacement=1.183 in | Max Plastic Strain=27.44

Figure 5: Case 4 Impact Region Out-of-Plane Displacement and Plastic Strain

Case 5: Four Layers with a Quarter-Inch Gap

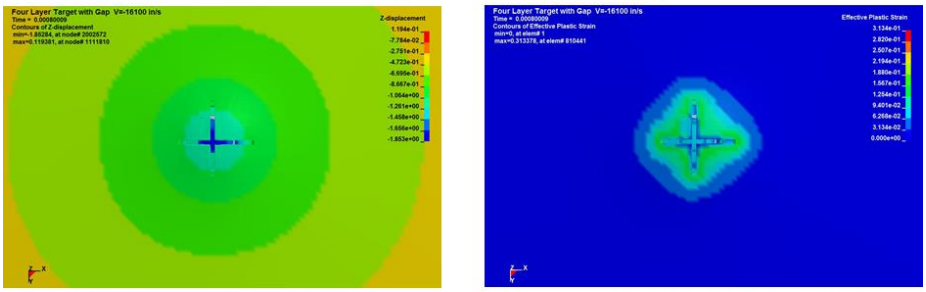

Max Z-Displacement=1.853 in | Max Plastic Strain=31.34

Figure 6: Case 5 Impact Region Out-of-Plane Displacement and Plastic Strain

Case	Perforation Velocity (in/s)	Max Plastic Strain	Max Z-Displacement (in)
1	18170	25.28	0.654
2	**19870**	**28.28**	**1.662**
3	16660	26.69	1.518
4	16110	27.44	1.183
5	16100	31.34	1.853

Table 2: Comparison of Perforation Velocity, Maximum Plastic Strain, and Maximum Out-of-Plane Displacement in the Impact Region

The total internal energy (the sum of the internal energy of all of the target layers) is plotted versus time in Figure 7. These results show that Cases 2 and 5 have the highest internal energy for the impact event, which is consistent with those cases also having the highest plastic strain and out-of-plane displacements.

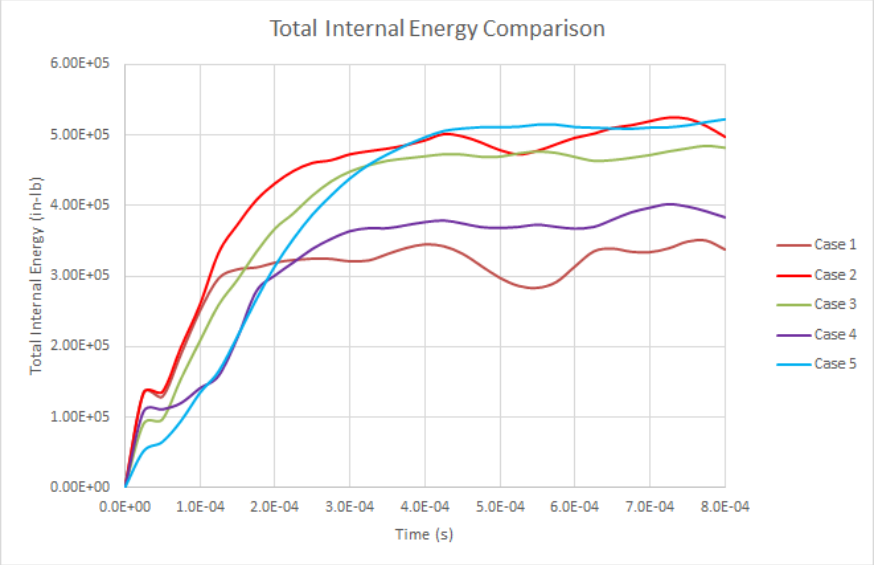

Figure 7: Total Internal Energy Comparison

Future Work

Future work will be aimed at gaining a better understanding of the trend in the results by closer examination of the triaxiality and Lode parameters for failed elements to determine the predominant failure mode for each of the configurations. Additional studies, varying the size of the spherical projectile and its angle of incidence with the target, will also be completed. Finally,

comparisons with other projectile geometries, including a flat plate and a conical shape, will also be completed.

Acknowledgments

I want to acknowledge the assistance of Dr. Sean Haight, for guidance on the material-model theoretical development and the titanium-6Al-4V input generation; Dr. Kelly Carney, for general discussions on the analyses and results; and Dr. Anthony Dennis, for initially recommending the study.

References

[1] Hagg, A.C. and Sankey, G.O., "The Containment of Disk Burst Fragments by Cylindrical Shells," ASMW Paper 73-WA-Pwr-2, December 1973.

[2] Stamper, E. and Hale, S., "The Use of LS-DYNA Models to Predict Containment of Disk Burst Fragments," 10th International LS-DYNA Users Conference, Detroit, 2008.

[3] Hu, S., Wu, C.T., and Guo, Y., "Engine Impeller Sub-fragmentation Simulation Using EFG Method," 11th International LS-DYNA Users Conference, Detroit, 2010.

[4] Carney, K., Pereira, M., Revilock, D., and Matheny, P., "Jet Engine Fan Blade Containment using Two Alternate Geometries," 4th European LS-DYNA Users Conference, Ulm, Germany, 2003.

[5] Emmerling, W., Altobelli, D., Carney, K., Pereira, M., "Development of a New Material Model in LS-DYNA, Part 1: FAA, NASA and Industry Collaboration Background," DOT/FAA/TC-13/25 P1, April 2014.

[6] Buyuk, M., "Development of a New Material Model in LS-DYNA, Part 2: Development of a Tabulated Thermo-Viscoplastic Material Model with Regularized Failure for Dynamic Ductile Failure Prediction of Structures Under Impact Loading," DOT/FAA/TC-13/25 P2, July 2014.

[7] Seidt, J., "Development of a New Material Model in LS-DYNA, Part 3: Plastic Deformation and Ductile Fracture of 2024 Aluminum under Various Loading Conditions," DOT/FAA/TC-13/25 P3, April 2014.

[8] Haight, S., "Development of a Titanium Alloy Ti-6Al-4V Material Model Used in LS-DYNA," DOT/FAA/AR-15/11, May 2015.